ELECTRICAL CHARACTERIZATIONS OF CdTe/CdS POLY-CRYSTALLINE THIN FILM SOLAR CELLS

CARACTERIZACIONES ELÉCTRICAS DE CELDAS SOLARES POLICRISTALINAS A CAPAS DELGADAS DE CdTE/CdS

O. Almora-Rodríguez,[a ‡] L. Vaillant[b †] and A. Bosio[c *]

a) Department of Physics, José A. Echeverría Higher Polytechnic Institute (ISPJAE) and ENERMAT Division, Institute of Materials Science and Technology (IMRE), University of Havana, Havana, Cuba; oalmora89@gmail.com‡
b) ENERMAT Division, Institute of Materials Science and Technology (IMRE) and School of Physics, University of Havana, Havana, Cuba; vaillant@fisica.uh.cu†
b) INFM- Physics Department, University of Parma, Parma, Italy; alessio.bosio@unipr.it*
† corresponding author

(Recibido 21/3/2014; Aceptado 20/10/2014)

CdTe/CdS poly-crystalline thin film solar cells are characterized by means of dark current-voltage (I-V) and capacitance-voltage (C-V) measurements, both as a function of temperature. The studied CdTe/CdS solar cells were fabricated using a novel gaseous thermal treatment in the presence of chloride. I-V curves analysis allows us to extract information about carrier transport phenomena as a function of temperature. From C-V curves we can obtain the doping profiles and analyze the traps levels distribution in the absorber material.

Se presentan caracterizaciones eléctricas de corriente-voltaje (I-V) y capacidad voltaje (C-V) en oscuridad y en función de la temperatura, realizadas a celdas solares policristalinas a capas delgadas basadas en CdTe/CdS. Durante la fabricación de los dispositivos estudiados se utilizó un tratamiento térmico novedoso con presencia de cloro en fase gaseosa. La respuesta I-V permitió analizar los mecanismos de transporte en función de la temperatura. A partir de las mediciones de C-V se obtuvieron los perfiles de concentración de portadores y se analiza la distribución de trampas en el CdTe.

PACS: Thin films electrical properties of, 73.61.Ga; Thin film III-V and II-VI solar cells, 88.40.jm; Transport processes in thin films, 73.50.-h, 73.61.-r; Doping profiles, 61.72.U-, 81.70.Jb; Deep energy levels, 71.55.-I; Defect levels bulk matter, 71.55.-I.

INTRODUCTION

CdTe/CdS thin films solar cells are still an actual and promising device in photovoltaic due to its perspectives in performance improvement and low cost.

Actually, the interest on these devices seems to renew, well after ten years without an official reported efficiency record, since from October of 2010 to August of 2014 seven for modules and six for cells were publicized [1-12]. The most recent records were for First Solar with efficiencies of 17.5% and 21.0% for laboratory modules and cells respectively [8,12].

Thin film CdTe solar cells are formed by the TCO/ buffer layer/ CdS/ CdTe/ back contact superposition of layers over a substrate in the superstrate configuration. Here, p-type CdTe plays a fundamental function as absorbing material. n-type CdS film complete the p-n junction as the traditional partner for CdTe-based solar cell.

After years of research some key problems remain concerning the current investigations. Among them, it can be mentioned the poly-crystalline nature of the layers, the difficulty to develop stable and ohmic back contacts and the role of the thermal treatment (TT) in the presence of Cl.

In particular, the TT in presence of Cl has been considered for several years as a magical step in the fabrication of CdTe/CdS solar cells [13][12]. Since CdTe and CdS have a lattice mismatch of 9.7% [14], the main interface created between this two materials was not supposed to be optimal. In agreement with this, the cells fabricated without further annealing had a poor performance. However, after the introduction of the TT in 1985 [15], the treated cells crossed the frontier of 11% conversion efficiency [16].

For the TT the most common procedure is to growth a $CdCl_2$ layer on top of the CdTe surface, then heat the structure between 350°C and 400°C, and finally to practices a chemical etching in nitric + phosphoric acid solution (usually called NP solution). The chemical etching is made for cleaning and for making the CdTe surface Te-rich prior the back contact deposition [17, 18]. In a complete dry fabrication process this last wet step means a disadvantage for industrial scale develop, due to the need of introducing the expensive recycling system for the derived chemical residuals.

The devices studied in this work are fabricated in a complete dry and industrially scalable process. For this purpose, an alternative method for the TT based in an entire vapor phase process was developed [19-21]. This basically consists in heating the structure in the presence of HCF_2Cl gas during times ranging on the order of minutes. Finally, vacuum is applied to re-evaporate possible $CdCl_2$ remainders, leaving the

CdTe surface ready for the back contact layer deposition.

In order to characterize CdTe/CdS solar cells treated with this alternative annealing the dark current-voltage (I-V) and capacitance-voltage (C-V) characteristics were considered, both as a function of temperature. Dark I-V curves allow us to investigate aspects related to the transport phenomena and C-V about the doping profiles and the presence of trap levels. These characterizations, mainly C-V, varying temperature are not frequently found in literature.

EXPERIMENTAL

The substrates used in the studied structure were soda-lime glasses of 2.5 cm^2. Prior the cell fabrication the substrates are cleaned by submerging them in acetic acid, later in a solution of ethyl alcohol and nitric acid (with volumetric proportions of 1:3), and finally in a mixing of propanol and acetone. For the front contact fabrication the TCO was ITO and ZnO was introduced as the buffer layer. Both materials were deposited with direct current (DC) magnetron sputtering technique. For ITO deposition the substrate temperature was of 400°C - 450°C and the inert atmosphere was of 10^{-3} mbar of Ar with presence of oxygen in the chamber. The resulting film thickness was of about 1.0 μm. Similar parameters, but dispensing with the oxygen presence, were required for the ZnO layer.

Once the fabrication of the front contact was done, the structure was placed in the radio frequency (RF) magnetron sputtering system for the CdS film deposition. In this case were also used 10^{-3} mbar of Ar atmosphere, but this time with the inclusion of CHF_3 in the atmosphere composition of the chamber. The substrate temperature was kept at 220°C and the thickness of the films was around 0.05 μm.

Subsequently, the CdTe layer fabrication was done by Close-Spaced Sublimation (CSS). In this step was used an atmosphere of pure Ar in the CSS chamber and the temperatures for the source and the substrate were about 570°C - 590°C and 510°C - 530°C, respectively. The resulting films presented thickness between 10 - 15 μm and columnar oriented grains with sizes near the 20 μm in the perpendicular sense of the light path.

For our novel TT the grown structure was located in the furnace chamber where the initial vacuum reached 10^{-6} mbar. After heating, the temperature was established around the 400°C. Later the compositions of HCF_2Cl and Ar of 20 - 100 mbar and 800 - 900 mbar, respectively, were introduced in the chamber. Then the structure was treated during times between 2 and 10 minutes. After TT was practiced vacuum during 10 minutes for re-evaporate probable $CdCl_2$ remainders.

The two back contact constituent layers (Sb_2Te_3 and Mo) were fabricated once more using the RF magnetron sputtering, with 10^{-3} mbar of Ar pressure and substrate temperature of 400°C. The thickness of the complete back contact film was evaluated in 0.1 μm. Following, the light soaking process was practiced leaving the cells for several hours under 10 or more suns at temperatures higher than 100°C without observing degradation.

All the pressure measurements and controlling were performed by a Varian MultiGauge. The fabricated cells studied in this work reported efficiencies of 10.6-13.3% with active areas of 1.57 - 1.74 cm^2. More information about the fabrication process can be found in [21].

The experimental characterization set up for I-V and C-Vwas based on the S4600 Modular DLTS System, of Bio-Rad Polaron Equipment Ltd., with the support of other equipments. This system is provided with a cryostat with re-flowing liquid nitrogen to vary and measure temperatures between 87 and 310 K, the power supply and the capacitance meter Boonton 72B. To measure the bias applied was used an ISM 110 of Gantner Instruments. The current measurements for the I-V and the voltage from the capacitance meter for the C-V were performed by the multimeter Keithley 2001. For the measurement and primary calculating processes an automation software done with the LabView 7.1 programming tool was developed. The determination of the cells areas was performed by processing digital images (4800 DPI) of the samples with the software Digimizer 3.7. The cross sections of the cells were observed through microscopic images taken with a SEM Vega 3 Tescan. Further specifications about the characterization system can be consulted in [22].

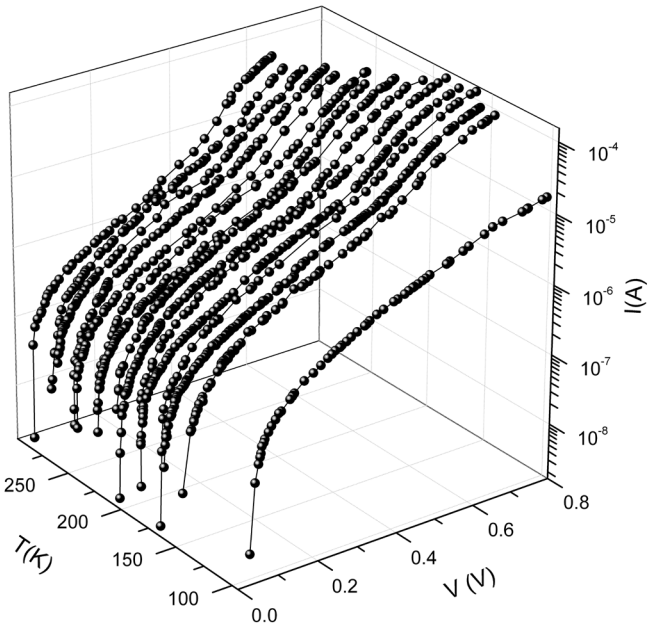

Figure 1: Dark I-V for different temperatures of one cell of the ensemble with logarithmic current scale. The behavior presented is typical for a semiconductor diode.

DARK I-V MEASUREMENTS AS A FUNCTION OF TEMPERATURE

For showing the results an ensemble of four cells denominated 1, 2, 3 and 4 was selected, whose times of TT were 2, 5, 6 and 10 minutes respectively. This set of samples will allow us to compare results with earlier studies [20, 21] on cells treated

with approximately the half of pressure in the chamber.

Dark I-V characteristic behavior for the four cells presented the typical performance of a semiconductor diode [23], as it is shown in figure 1. The recombination-generation current region is displayed as the best defined, while the diffusion-current and high injection regions presented a slight trend to overlapping with the decrease of temperature.

Some differences in the evolution of the I-V curves with the temperature can be better appreciated in the linear scale, as it is shown in figure 2. The remarkable increase of the curves slope with temperature in the high voltage region suggests the decrease of series resistance (R_s) with the rise of temperature. The nature of this behavior responds to the predominant resistive element in the entire structure. In this sense the most likely factors to consider are the bulk of CdTe and the back contact. The bulk of CdTe occupy nearly the entire volume of the cell and its carrier concentration is significantly lower. On the other hand the back contact is known by its current rectifying effect for forward bias.

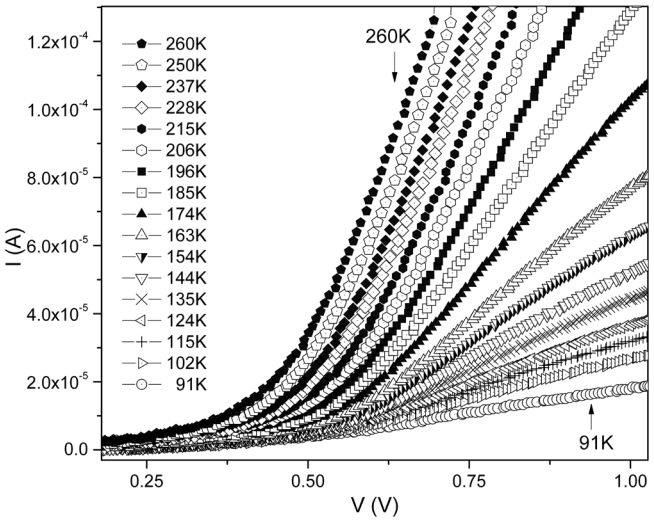

Figure 2: Dark I-V for different temperatures of one cell with linear current scale. The change of slope with temperature for high forward bias region means change of R_s.

By calculating R_s using the graphic method [22] and plotting the values versus temperature it results in the exponential decay of $R_s(T)$ as it is displayed in figure 3. This behavior can be explained assuming that the transport over the back contact barrier follows the thermoionic emission. This accepted assumption [24, 25] considers as negligible the tunneling through the back contact barrier. In order to support this last statement the width of the back contact space charge region in forward bias were calculated via C-V characteristics (see following section) resulting significantly large values.

Aiming to calculate the potential barrier height associated to the back contact, the experimental data was fitted to the equation 1 as shown in figure 3 with discontinues (red) curves (the region of lows R_s and high temperatures is best represented in the insert).

$$R_s(T) = R_{\Omega 0} + \frac{\partial R_{s\Omega}}{\partial T} T + R_{sk} e^{\frac{\Phi_{sk}}{kT}} \quad (1)$$

In this expression $R_{\Omega 0}$ is the ohmic resistance at 273 K, Φ_{sk} is the Schottky potential barrier of the contact, R_{sk} is a fitting parameter and $\partial R_{s\Omega} / \partial T$ carry implicit the influence of the rest contributing series resistances in the device. This last linear coefficient is called ohmic coefficient by D. L. Bätzner et al in [24].

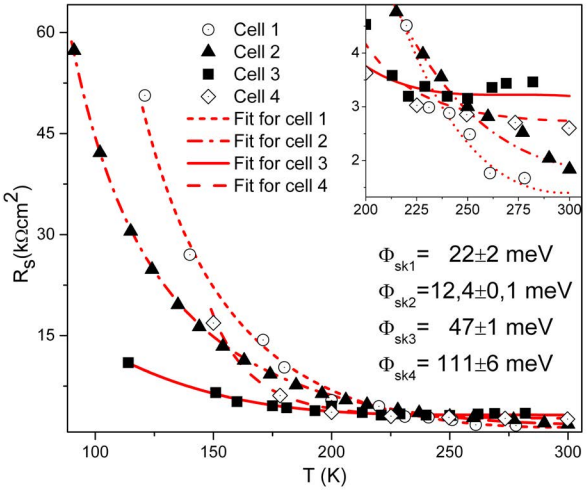

Figure 3: $R_s(T)$ scattering with respective fitting curves and barriers heights Φ_{ski} for the four cells. Insert: region of lows R_s and high temperatures.

The Φ_{sk} calculated values, displayed in figure 3, are of the thermal voltage order, which means an acceptable level of back contact resistive effects. In other words, it is possible to analyze in a good approximation other aspects of the cell, such as the main junction, by neglecting the back contact influence.

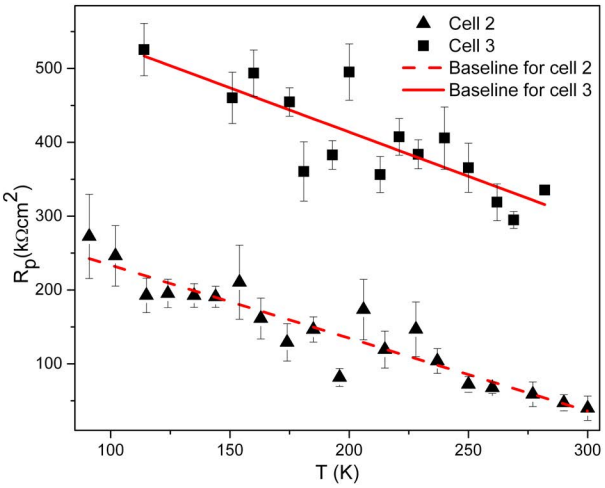

Figure 4: $R_{sh}(T)$ plots with respective linear fitting as baselines for two cells of the ensemble. This linear trend is produced by re-combinative effects.

The shunt resistance (R_{sh}) and the ideality factor (n) were also calculated for these cells. The $R_{sh}(T)$ plots shown in figure 4 displays a linear decrease with temperature, which correspond to an increase of leakage currents with temperature. In this graph the linear behavior is emphasize by the corresponding

linear fitting curves that serve as baselines. This sort of tendency can be explained as a consequence of re-combinative effects in the low voltage region [26].

The Arrhenius plot displayed in figure 5 was elaborated for the analysis of n. Two remarkable characteristics predominate in that graph: the decrease of n with temperature and its values, higher than 2 practically for all of them. In CdTe/CdS devices these features suggest the prevailing of tunneling as a transport mechanism through the main junction [27]. A third characteristic is shaded in gray, which was the change in slope presented by all the cells around the 205 K; that is interpreted as a change in the main transport mechanisms at that temperature [24]. In our case this change may well be from the tunneling, at low temperatures, to recombination in the depletion region, at high temperatures [22].

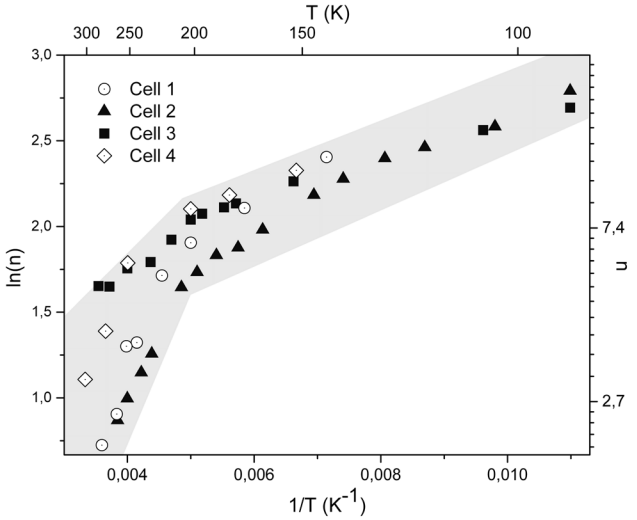

Figure 5: Arrhenius plot of *n* for the four cells. The presented change of slope trend is shaded evidencing a change of main transport mechanisms.

C-V MEASUREMENTS AS A FUNCTION OF TEMPERATURE

C-V characteristics were performed always while decreasing the AC voltage and with a constant frequency of 1 MHz. These are aspects to attend due to the hysteresis effects always present in the capacitance studies [28].

The measurements are presented in the typical Mott-Schottky-plots, as displayed in figure 6 for one cell of the ensemble. The non-linearity of this curves evidence the strong presence of trap levels in the forbidden band of CdTe. Moreover, these kinds of irregularities make physically senseless the calculus of the majority carriers density and the built in potential by the model of the abrupt junction [23]. A correction to this model in such conditions has been proposed earlier [28] with the introduction of an intrinsic region inside the depletion region. The space charge region would have then a transition region where the majority carriers concentrations would vary between the intrinsic part, located next the juncture, and the concentration value in the border of the depletion region.

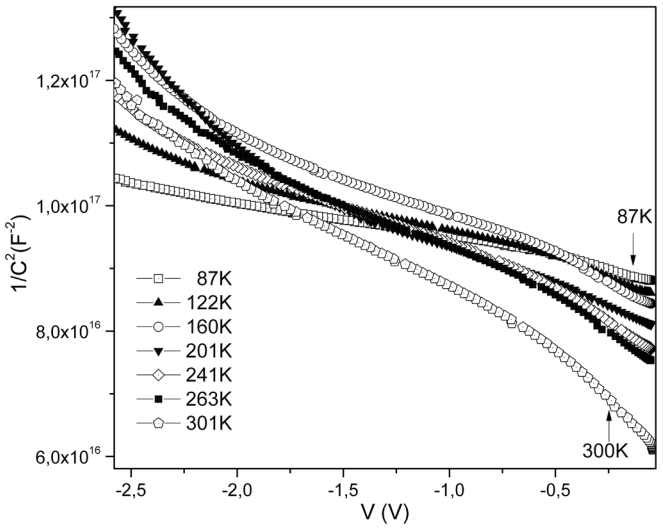

Figure 6: Mott-Schottky-plots for different temperatures of one cell of the ensemble. Nonlinearity of plots evidences strong presence of defect levels.

The *apparent* carrier concentration[1] is shown in figure 7. As it can be seen, the depletion region width is between 4-5 μm at zero bias, which is about a third of the CdTe layer length (10-15 μm).

The rising in dopant concentration, around 4.0-4.5 μm from the junction, precedes two maxima (best represented in figure 7 insert). This increasing in holes concentration evidences the presence of the above mentioned transition region between the intrinsic layer and the border of the depletion region [28]. The two maxima can be explained as a consequence of a distribution of emitting carriersbroad level bands. The presence of broad level bands in CdTe forbidden band is a topic widely handled in the literature [29, 30].

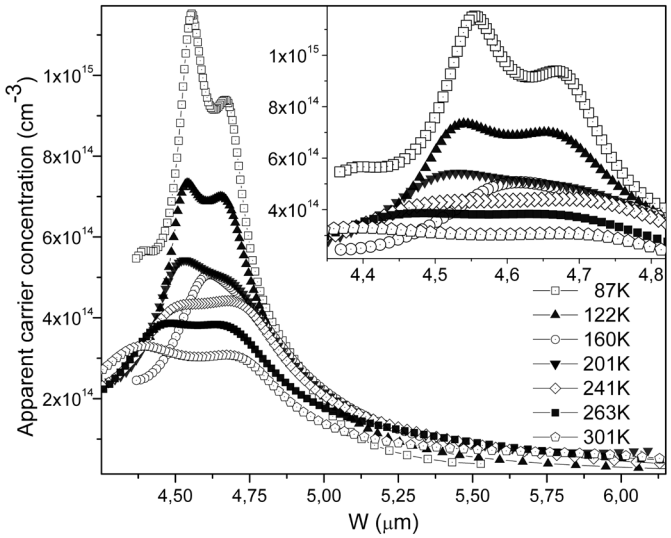

Figure 7: Doping profiles (measured from the CdTe/CdS junction) for different temperatures of the cell whose Mott-Schottky-plots are displayed in figure 6. Insert: holes concentration maxima region.

Another thing to underline was the curves decays, around 4.7–6.0 μm from the junction. That sort of holes apparent

1 For an explicit explanation of the apparent carrier concentration calculus and meaning can be consulted [22, 23, 27].

concentration decreasing with the rise of the depletion layer could be explained as the result of the Cd vacancies (V_{Cd}) passivation process during the TT. As is known the CdTe layer conductivity is defined by the V_{Cd} concentration, which is the most extended defect in the material. The Cl atoms interact with the CdTe surface during the TT, and are considered responsible of the V_{Cd}-Cl complex defect formation. That's why is expected a gradient in holes concentration produced by the penetration of Cl atoms.

If the back contact junction is considered, the trend to carrier concentration reduction produced by the passivation process implies a large depletion region. Focused on the two diode model [27, 31, 32], the depletion regions widths for the back contact diodes were calculated. The followed procedure was the same already mentioned for the doping profiles, but in this case, instead of analyze the C^{-2}-V curves with reverse bias, the calculus were done at the high forward bias region of the analogue Mott-Schottky-plots. The obtained values of 3-4 μm, as have been already referred, reflect a detriment factor for tunneling through the back contact barrier, and so for the ohmic behavior.

In earlier studies [20, 21] CdTe/CdS cells were fabricated using this phase vapor TT but treated with approximately the half of the pressure in the chamber. Making a comparison, the devices exhibit similar I-V characteristics but however, differences in the apparent carrier concentration behavior. The less pressurized TT cells did not present the distribution of maxima nor the decreasing trend toward the back contact. Thus, we can think that by raising the pressure at the chamber the V_{Cd} passivation process was intensified and the defect levels distribution was redistributed generating broader level bands. For those devices, chloride was considered to contribute to the pasivation of the cadmium vacancies (V_{Cd}) recombination centers, by the formation of A-centers $(Cl^{-} - V_{Cd}^{+})^{0}$ [33].

CONCLUSION

CdTe/CdS polycrystalline photovoltaic cells fabricated with a novel phase vapor TT were characterized by I-V and C-V techniques, both as a function of temperature. The study of transport phenomena by the I-V characteristics exhibited the dominance of the generation-recombination process for the region of low forward bias, and the significant series resistance dependence with temperature for high forward bias due to the back contact rectifying barrier. The Mott-Schottky-plots from C-V characteristics evidenced the strong presence of defect levels and the doping profiles shown a relative large width of the depletion layer. Also, with the apparent carrier concentration graph, was displayed the formation of emitting carriers broad level bands and the effect of V_{Cd} passivation during the TT.

[1] M. A. Green et al., Prog. Photovolt. Res. Appl. **18**, 346 (2010).
[2] M. A. Green et al., Prog. Photovolt. Res. Appl. **19**, 84 (2011).
[3] M. A. Green et al., Prog. Photovolt. Res. Appl **19**, 565 (2011).
[4] M. A. Green et al., Prog. Photovolt. Res. Appl. **20**, 12 (2012).
[5] M. A. Green et al., Prog. Photovolt. Res. Appl. **20**, 606 (2012).
[6] M. A. Green et al., Prog. Photovolt. Res. Appl., 21, 1 (2013).
[7] M. A. Green et al., Prog. Photovolt. Res. Appl. **21**, 827 (2013).
[8] M. A. Green et al., Prog. Photovolt. Res. Appl. **22**, 701 (2014).
[9] http://files.shareholder.com/downloads/FSLR/2191222229x0x533696/bf593fda-83ac-4cd1-bfc5-43bd49a72648/FSLR_News_2012_1_16_English.pdf http://investor.firstsolar.com/releasedetail.cfm?ReleaseID=833971 http://investor.firstsolar.com/releasedetail.cfm?releaseid=743398 http://investor.firstsolar.com/releasedetail.cfm?ReleaseID=864426
[10] B. M. Basol, Int. J. Sol. Energy **12**, 25 (1992).
[11] R. H. Bube, *Photovoltaic Materials* (Imperial College Press, London, 1998), p. 136.
[12] B. M. Basol et al., J. Appl. Phys. **58**, 3809 (1985).
[13] K. Zweibel et al., "Progress and Issues in Polycrystalline Thin-Film PV Technologies", 25th IEEE Photovoltaic Specialists Conference(IEEE Publishing, NY, 1996), p. 745.
[14] A. Romeo et al., Prog. Photovolt: Res. Appl. **12**, 93 (2004).
[15] Xiaonan Li et al., J. Vac. Sci. Technol. A **17**, 805 (1999).
[16] N. Romeo et al., 21st European Photovoltaic Solar Energy Conference, 1857, 2006.
[17] L. Vaillant et al., Thin Solid Films **516**, 7075 (2008).
[18] L. Vaillant, "Sobre las propiedades optoelectrónicas de celdas solares de CdTe/CdS", PhD Thesis, University of Havana, Cuba, 2008.
[19] O. Almora-Rodríguez, "Caracterizaciones eléctricas de celdas fotovoltaicas de CdTe/CdS", Diploma Thesis, University of Havana, Cuba, 2013.
[20] S. M. Sze and Kwok K. Ng, *Physics of semiconductor devices*, 3rd Ed. (John Wiley & Sons Inc., New Jersey, 2007), pp. 96-98.
[21] D. L. Bätzner et al., Thin Solid Films **261**, 288 (2000).
[22] S.H. Demtsu and J.R. Sites, Thin Solid Films **510**, 320 (2006)
[23] M. García, M. Iglesias and S. Aguilera, Rev. Cub. Fís. **12**, 170 (1992).
[24] J. Poortmans and V. Arkhipov, *Thin Film Solar Cells Fabrication, Characterization and Applications* (John Wiley & Sons Ltd, England, 2006), pp. 277-324.
[25] P. H. Mauk et al.,IEEE T. Electron. Dev. **37**, 422 (1990).
[26] U. Reislöhne et al., Thin Solid Films **515**, 6175 (2007).
[27] A. E. Rakhshani and Y. Makdisi, Phys. Stat. Sol. (a) **179**, 159 (2000).
[28] A. Niemegeers and M. Burgelman, J. Appl. Phys. **81**, 2881 (1997)
[29] M. Burgelman et al., Appl. Phys. A **69**, 149 (1999).
[30] N. Romeo et al., Sol. Energ. Mat. Sol. C. **94**, 2 (2010).